The Complex Wave Representation of Distance Transforms

Karthik S. Gurumoorthy, Anand Rangarajan and Arunava Banerjee

Department of Computer and Information Science and Engineering,
University of Florida, Gainesville, FL, USA
{ksg,anand,arunava}@cise.ufl.edu

Abstract

The complex wave representation (CWR) converts unsigned 2D distance transforms into their corresponding wave functions. The underlying motivation for performing this maneuver is as follows: the normalized power spectrum of the wave function is an excellent approximation (at small values of Planck's constant—here a free parameter τ) to the density function of the distance transform gradients. Or in colloquial terms, *spatial frequencies are gradient histogram bins*. Since the distance transform gradients have only orientation information, the Fourier transform values mainly lie on the unit circle in the spatial frequency domain. We use the higher-order *stationary phase approximation* to prove this result and then provide empirical confirmation at low values of τ. The result indicates that the CWR of distance transforms is an intriguing and novel shape representation.

Key words: distance transforms, Voronoi, Hamilton-Jacobi equation, Schrödinger wave function, complex wave representation (CWR), stationary phase (method of), gradient density, power spectrum

1 Introduction

Over the past three decades, image analysis has borrowed numerous formalisms, methodologies and techniques from classical physics. These include variational and level-set methods for active contours and surface reconstruction [1, 12], Markov Chain Monte Carlo (MCMC) [17], mean-field methods in image segmentation and matching [9, 20, 8], fluidic flow formulations for image registration [6] etc. Curiously, there has been very little interest in adapting approaches from quantum mechanics. This is despite the fact that *linear* Schrödinger equations are the quantum counterpart to *nonlinear* Hamilton-Jacobi equations [4] and the knowledge that the quantum approaches the classical as Planck's constant $\hbar$ tends to zero [2].

The principal theme in this work is the introduction of complex wave representations (CWRs) of shapes. We begin by reconstructing the well known bridge between the Hamilton-Jacobi and Schrödinger equations as adapted to the problem of Euclidean distance transform computation. As expected, the familiar nonlinear, static Hamilton-Jacobi equation emerges from a linear, static Schrödinger equation in the limit as $\tau \to 0$. This paves the way for the *complex wave representation* (CWR) of distance transforms: here the wave function $\psi(x, y)$ is equal to $\exp\left\{i\frac{S(x,y)}{\tau}\right\}$ where $S(x, y)$ is the distance transform in 2D.

Since distance transform gradients (when they exist) are unit vectors [13], their appropriate representation is the space of orientations. The *centerpiece of this work* is the following statement

of equivalence: $|\Psi_\tau(u(\theta), v(\theta)|^2$—the squared magnitude of the normalized Fourier transform of $\psi(x, y)$ is approximately equal to the density function of distance transform gradients with the approximation becoming increasingly accurate as τ tends to zero. We will prove this conjecture using the stationary phase approximation [11]—a well known technique in asymptotic analysis. The significance for shape analysis is that *spatial frequencies become histogram bins*. This result also demonstrates that the well known interpretation of the squared magnitude of the wave function as a probability density [2] is not merely a philosophical position. Instead, the squared magnitude of the wave function (in the spatial frequency basis) is shown to be an approximation to the distance transform gradient density (with the approximation becoming increasingly accurate as $\tau \to 0$).

2 The Complex Wave Representation (CWR)

We begin with Euclidean distance functions—more popularly referred to as distance transforms. Since distance transforms are used to set up the transition from Hamilton-Jacobi to Schrödinger wave functions, we stick with the simplest case: *unsigned* distance functions of a point-set. Given a point-set $\left\{Y_k \in \mathbb{R}^D,\, k \in \{1, \ldots, K\}\right\}$, the distance transform is defined as

$$S(x) \stackrel{\text{def}}{=} \min_{\{Y_k\}} \|x - Y_k\| \tag{1}$$

where $x \in \Omega$, is a bounded domain in $\mathbb{R}^D$. Below, we mainly use $D = 2$. In computational geometry, this is the Voronoi problem [15, 7] and the solution $S(x)$ can be visualized as a set of cones (with the centers being the point-set locations $\{Y_k\}$). The distance transform $S(x)$ is not differentiable at the point-set locations and at the Voronoi boundaries but satisfies the static, nonlinear Hamilton-Jacobi equation [13, 16]

$$\|\nabla S(x)\| = 1 \tag{2}$$

elsewhere. Furthermore $S(x) = 0$ at the point-set locations.

The intimate relationship between the Hamilton-Jacobi and Schrödinger equations is well known in theoretical physics [4] and leveraged by our previous work on this topic [14]. For our purposes, the static, *nonlinear* Hamilton-Jacobi equation can be embedded in a static, *linear* Schrödinger equation. Consider the following linear differential equation

$$-\tau^2 \nabla^2 \psi(x) = \psi(x) \tag{3}$$

where $\psi(x)$ is a complex wave function and τ a free parameter (usually Planck's constant in the physics literature). Now, substitute $\psi(x) = \exp\left\{i\frac{S(x)}{\tau}\right\}$ with the notation $S(x)$ deliberately chosen to resonate with the distance transform above. We get using simple algebra [5]

$$\|\nabla S(x)\|^2 - i\tau \nabla^2 S(x) = 1 \tag{4}$$

which approaches (3) as $\tau \to 0$ provided $|\nabla^2 S(x)|$ is bounded. Due to this equivalence, and since the focus in this work is not on efficient computation of $S(x)$, we will henceforth not make a distinction between the Hamilton-Jacobi field $S(x)$ and the phase of the wave function $\psi(x)$.

We have shown—following the theoretical physics literature and our previous work in EMM-CVPR 2009 [14]—that the static, linear Schrödinger equation in (3) is capable of *expressing* the static, nonlinear Hamilton-Jacobi equation in (2). The focus in this work, however, is on leveraging the complex wave representation (CWR) $\psi(x) = \exp\{i\frac{S(x)}{\tau}\}$.

3 Distance transform gradient density

The geometry of the distance transform in 2D corresponds to a set of intersecting cones with the origins at the Voronoi centers [7]. The gradients of the distance transform (which exist globally except at the cone intersections and origins) are unit vectors and satisfy $\| \bigtriangledown S\| = 1$. Therefore the gradient density function is one dimensional and defined over the space of *orientations*. The orientations are constant and unique along each ray of each cone. Its probability distribution function is given by

$$F(\theta \leq \Theta \leq \theta + \Delta) \equiv \frac{1}{L} \int \int_{\theta \leq \arctan\left(\frac{S_y}{S_x}\right) \leq \theta + \Delta} dxdy \tag{5}$$

where we have expressed the orientation random variable—$\Theta = \arctan\left(\frac{S_y}{S_x}\right)$—as a random variable transformation of a uniformly distributed random variable (defined on a bounded 2D domain). The probability distribution function also induces a *closed-form expression* for its density function as shown below.

Let Ω denote the polygonal grid. Let $L = \mu(\Omega)$ represent the area of the grid and $l = \sqrt{L}$. Let $Y = \{Y_k \in \mathbb{R}^2, k \in \{1, \ldots, K\}\}$ be the given point-set locations. Then the Euclidean distance transform at a point $X = (x, y) \in \Omega$ is given by

$$S(X) \equiv \min_k \|X - Y_k\| = \min_k (\sqrt{(x - x_k)^2 + (y - y_k)^2}). \tag{6}$$

Let $\mathcal{D}_k$, *centered* at Y_k, denote the k^{th} Voronoi region corresponding to the input point Y_k. $\mathcal{D}_k$ can be represented by the Cartesian product $[0, 2\pi) \times [0, R_k(\theta)]$ where $R_k(\theta)$ is the length of the ray of the k^{th} cone at orientation θ. If a grid point $X = (x, y) \in Y_k + \mathcal{D}_k$, then $S(X) = \|X - Y_k\|$. Each $\mathcal{D}_k$ is a convex polygon whose boundary is composed of a finite sequence of straight line segments. Even for points that lie on the Voronoi boundary–where the radial length equals $R_k(\theta)$–the distance transform is well defined. The area L of the polygonal grid Ω is given by

$$L = \sum_{k=1}^{K} \int_0^{2\pi} \int_0^{R_k(\theta)} r dr d\theta = \sum_{k=1}^{K} \int_0^{2\pi} \frac{R_k^2(\theta)}{2} d\theta. \tag{7}$$

With the above set-up in place and by recognizing the cone geometry at each Voronoi center Y_k, equation (5) can be simplified as

$$F(\theta \leq \Theta \leq \theta + \Delta) \equiv \frac{1}{L} \sum_{k=1}^{K} \int_\theta^{\theta+\Delta} \int_0^{R_k(\theta)} r dr d\theta = \frac{1}{L} \sum_{k=1}^{K} \int_\theta^{\theta+\Delta} \frac{R_k^2(\theta)}{2} d\theta. \tag{8}$$

Following this drastic simplification, we can write the closed-form expression for the density function of the unit vector distance transform gradients as

$$P(\theta) \equiv \lim_{\Delta \to 0} \frac{F(\theta \leq \Theta \leq \theta + \Delta)}{\Delta} = \frac{1}{L} \sum_{k=1}^{K} \frac{R_k^2(\theta)}{2}. \tag{9}$$

Based on the expression for L in (7) it is easy to see that

$$\int_0^{2\pi} P(\theta) d\theta = 1. \tag{10}$$

Since the Voronoi cells are convex polygons [7], each cell contributes exactly one conical ray to the density function on orientation.

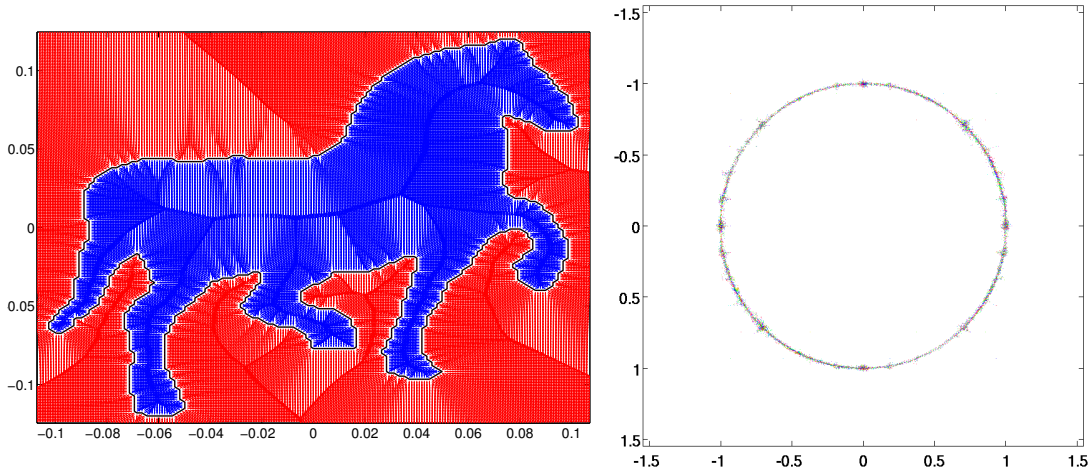

Figure 1: Left: Distance transform and gradient map of horse silhouette ($\tau = 0.00004$). Right: The scaled and normalized Fourier transform $\Psi_\tau(u, v)$. Please ZOOM into the plots (especially the horse silhouette) to see greater detail.

4 Properties of the Fourier transform of the CWR

4.1 Spatial frequencies as gradient histogram bins

Now, consider the CWR of the distance transform in 2D. We therefore use $\psi(x, y) = \exp\left\{i\frac{S(x,y)}{\tau}\right\}$ and $S(x, y)$ the actual distance transform of a point-set. We take its 2D scaled Fourier transform:

$$\Psi_\tau(u, v) = \frac{1}{2\pi\tau}\int\int_\Omega \exp\left\{i\frac{S(x, y)}{\tau}\right\}\exp\left\{-i\frac{ux + vy}{\tau}\right\}dxdy. \tag{11}$$

We see in Figure 1 (the figure on the right) that the Fourier transform values lie mainly on a circle and we have observed that this behavior tightens as $\tau \to 0$. The preferred theoretical tool in the literature to analyze this general type of behavior is the *stationary phase approximation* [11]—well known in theoretical physics but not so well known in image analysis. Below, we give a very brief and very qualitative exposition.

Consider the following integral (in 1D):

$$\int_{-\infty}^{\infty}\exp\left\{i\frac{f(x)}{\tau}\right\}\exp\left\{-i\frac{\nu}{\tau}x\right\}dx \tag{12}$$

where $f(x)$ is a twice differentiable function and ν a fixed parameter. The first exponential is a varying complex "sinusoid" whereas the second is a fixed complex sinusoid at frequency $\frac{\nu}{h}$. When we multiply these two complex exponentials, at low values of τ, the two sinusoids are usually not "in sync" and cancellations occur in the integral. Exceptions to the cancellation happen at locations where $f^{'}(x) = \nu$, since around these locations, the two sinusoids are in perfect sync (with the approximate duration of this resonance dependent on $f^{''}(x)$. The value of the integral is approximately

$$\sqrt{2\pi\tau}\exp\left\{\pm i\frac{\pi}{4}\right\}\sum_{\{x_0\}}\frac{1}{\sqrt{|f^{''}(x_0)|}}\exp\left\{i\frac{f(x_0) - \nu x_0}{\tau}\right\} \tag{13}$$

where $\{x_0\}$ is the set of locations at which $f^{'}(x_0) = \nu$. The approximation is increasingly tight as $\tau \to 0$. For more information, please see [11]. The stationary phase approximation gives a

theoretical explanation for the Fourier transform of $\psi(x,y)$ taking values mainly on the unit circle. In 2D, the stationary phase approximation indicates that the two sinusoids are in sync when $\nabla S = \nu$ where ν is now a 2D spatial frequency pair (u,v). However, since $\|\nabla S\| = 1$, strong resonance occurs only when $u^2 + v^2 = 1$ and when the distance transform orientation $\theta = \arctan\left(\frac{v}{u}\right)$. While this brief explanation does serious injustice to a vast topic, the important points nonetheless are: i) match between the orientation θ of each ray of the distance transform and the angle of the 2D spatial frequency $[\arctan\left(\frac{v}{u}\right)]$ and ii) match between the magnitude of ∇S (which is equal to one) and locations on the unit circle (corresponding to 2D spatial frequencies of magnitude one).

Next, we show that the squared magnitude of the Fourier transform (normalized such that it has overall unit norm) is approximately equal to the density function of the distance transform gradients.

4.2 Power spectrum of $\psi(x,y)$ as a gradient density estimator

The previous section motivated the use of the stationary phase approximation for evaluating integrals. In this section, we first outline the main result and then spend the remainder of the section proving it.

The main result: The squared magnitude of the Fourier transform of the complex wave representation $\psi(x,y) = \exp\left\{i\frac{S(x,y)}{\tau}\right\}$ is an increasingly more accurate approximation to the density function of ∇S as the free parameter τ tends to zero.

We now briefly outline the proof strategy: The Fourier transform of the CWR involves two spatial integrals (over x and y) which are converted into polar coordinate domain integrals. The squared magnitude of the Fourier transform involves multiplying the Fourier transform with its complex conjugate. The complex conjugate is yet another 2D integral which we will perform in the polar coordinate domain. Since the Fourier transform (suitable normalized) takes values very close to the unit circle, we then integrate the squared magnitude of the Fourier transform along the radial direction. This is a fifth integral. Finally, in order to eliminate unwanted phase factors, we first integrate the result of the above over very small angles and then take the limit as τ tends to zero. This integral and limit cannot be exchanged because the phase factors will not otherwise cancel. The remainder of this section mainly deals with managing these six integrals.

Define a function $F : \mathbb{R} \times \mathbb{R} \times \mathbb{R}^+ \to \mathbb{C}$ by

$$F(u,v,\tau) \equiv \frac{1}{2\pi\tau l} \int\int_{\Omega} \exp\left(\frac{iS(x,y)}{\tau}\right) \exp\left(\frac{-i(ux+vy)}{\tau}\right) dxdy. \tag{14}$$

For a fixed value of τ, define a function $F_\tau : \mathbb{R} \times \mathbb{R} \to \mathbb{C}$ by

$$F_\tau(u,v) \equiv F(u,v,\tau). \tag{15}$$

Observe that F_τ is closely related to the Fourier transform of $\exp\left(\frac{iS(x,y)}{\tau}\right)$ [3]. The scale factor $\frac{1}{2\pi\tau l}$ is the normalizing term such that $F_\tau \in L^2(\mathbb{R}^2)$ and $\|F_\tau\| = 1$.

Consider the polar representation of the spatial frequencies(u,v) namely $u = \tilde{r}\cos(\phi)$ and $v = \tilde{r}\sin(\phi)$ where $\tilde{r} > 0$. For $(x,y) \in Y_k + \mathcal{D}_k$, let $x - x_k = r\cos(\theta)$ and $y - y_k = r\sin(\theta)$ where $r \in (0, R_k(\theta)]$. Then

$$F_\tau(\tilde{r},\phi) = \sum_{k=1}^{K} C_k I_k(\tilde{r},\phi) \tag{16}$$

where

$$C_k = \exp\left(-\frac{i}{\tau}\left[\tilde{r}\cos(\phi)x_k + \tilde{r}\sin(\phi)y_k\right]\right) \tag{17}$$

and

$$I_k(\tilde{r},\phi) = \frac{1}{2\pi\tau l}\int_0^{2\pi}\int_0^{R_k(\theta)} \exp\left(\frac{i}{\tau}r\left[1-\tilde{r}\cos(\theta-\phi)\right]\right) r dr d\theta. \tag{18}$$

Lemma 1. *For $\tilde{r} \neq 1$, $\lim_{\tau\to 0} F_\tau(\tilde{r},\phi) = 0$.*

Proof. As each C_k is bounded, it suffices to show that if $\tilde{r} \neq 1$, then the limit $\lim_{\tau\to 0} I_k(\tilde{r},\phi) = 0$ for all I_k. Consider

$$I(\tilde{r},\phi) = \frac{1}{2\pi\tau l}\int_0^{2\pi}\int_0^{R(\theta)} \exp\left\{\frac{i}{\tau}r\left[1-\tilde{r}\cos(\theta-\phi)\right]\right\} r dr d\theta. \tag{19}$$

Let $p(r,\theta) = r(1-\tilde{r}\cos(\theta-\phi))$. Since we are interested only in the limit as $\tau \to 0$, essential contribution to $I(\tilde{r},\phi)$ in (19) comes only from the stationary points of $p(r,\theta)$ [10, 19]. The partial gradients of p are given by

$$\frac{\partial p}{\partial r} = 1-\tilde{r}\cos(\theta-\phi) \quad \frac{\partial p}{\partial \theta} = r\tilde{r}\sin(\theta-\phi). \tag{20}$$

The gradient equals zero only when $\tilde{r} = 1$ and $\theta = \phi$. Since $\tilde{r} \neq 1$ by assumption, no stationary points exist ($\bigtriangledown p \neq 0$). Then, using the two dimensional stationary phase approximation, we can show that $I = O(\tau)$ as $\tau \to 0$ and hence converges to zero in the limit as $\tau \to 0$. □

Define a function P_τ by

$$P_\tau(\tilde{r},\phi) \equiv |F_\tau(\tilde{r},\phi)|^2 = F_\tau(\tilde{r},\phi)\overline{F_\tau(\tilde{r},\phi)}. \tag{21}$$

By definition $P_\tau \geq 0$. Then, from basic algebra we have

$$\int_0^{2\pi}\int_0^{\infty} P_\tau(\tilde{r},\phi)\tilde{r}d\tilde{r}d\phi = 1 \tag{22}$$

independent of τ. Hence $\tilde{r}P_\tau(\tilde{r},\phi)$ can be treated as a density function irrespective of the value of τ. Furthermore, from Lemma (1), we see that as $\tau \to 0$, P_τ is concentrated only on the unit circle $\tilde{r} = 1$ and converges to zero everywhere else.

We now state and prove the main theorem in this work.

Theorem 2. *For any given $0 < \delta < 1$, $\phi_0 \in [0, 2\pi)$ and $0 < \Delta < 2\pi$,*

$$\lim_{\tau\to 0}\int_{\phi_0}^{\phi_0+\Delta}\int_{1-\delta}^{1+\delta} P_\tau(\tilde{r},\phi)\tilde{r}d\tilde{r}d\phi = \int_{\phi_0}^{\phi_0+\Delta} P(\phi)d\phi \tag{23}$$

where $P(\phi)$ is as defined in (9).

Proof. First observe that

$$\overline{F_\tau(\tilde{r},\phi)} = \sum_{k=1}^{K}\frac{\overline{C_k}}{2\pi\tau l}\int_0^{2\pi}\int_0^{R_k(\theta')} \exp\left(-\frac{ir'}{\tau}\left[1-\tilde{r}\cos(\theta'-\phi)\right]\right) r' dr' d\theta'. \tag{24}$$

$\overline{F_\tau(\tilde{r},\phi)}$ in (24) is the complex conjugate of the Fourier transform of the CWR in (14) and (15). Define

$$I(\phi) \equiv \int_{1-\delta}^{1+\delta} P_\tau(\tilde{r},\phi)\tilde{r}d\tilde{r}. \tag{25}$$

As $\tau \to 0$ $I(\phi)$ will approach the density function of the gradients of $S(x, y)$. Note that the integral in (25) is over the interval $[1-\delta, 1+\delta]$ where $\delta > 0$ can be made arbitrarily small (as $\tau \to 0$) due to Lemma (1). Since $P_\tau(\tilde{r}, \phi)$ equals $F_\tau(\tilde{r}, \phi)\overline{F_\tau(\tilde{r}, \phi)}$, we can rewrite $I(\phi)$ in (25) as

$$I(\phi) = \sum_{j=1}^{K}\sum_{k=1}^{K} \frac{1}{(2\pi\tau l)^2} \int_0^{2\pi}\int_0^{R_k(\theta')} \exp\left(\frac{-ir'}{\tau}\right) g_{jk}(r', \theta') r' dr' d\theta'. \tag{26}$$

Here

$$g_{jk}(r', \theta') \equiv \int_{1-\delta}^{1+\delta}\int_0^{2\pi}\int_0^{R_j(\theta)} \exp\left\{\frac{i}{\tau}\gamma_{jk}(r, \theta, \tilde{r}; r', \theta', \phi)\right\} f(r, \tilde{r}) dr d\theta d\tilde{r} \tag{27}$$

where

$$\gamma_{jk}(r, \theta, \tilde{r}; r', \theta', \phi) \equiv r\left[1 - \tilde{r}\cos(\theta - \phi)\right] + r'\tilde{r}\cos(\theta' - \phi) - \tilde{r}\rho_{jk} \tag{28}$$

and

$$\rho_{jk}(\phi) = \cos(\phi)(x_j - x_k) + \sin(\phi)(y_j - y_k) \tag{29}$$

with

$$f(r, \tilde{r}) = r\tilde{r}. \tag{30}$$

The main reason for rewriting $I(\phi)$ in this manner will become clear as we proceed. In (29),ρ_{jk} represents the phase term of the quantity $C_j\overline{C_k}$ with C_k defined earlier in (17). In the definition of $\gamma_{jk}(r, \theta, \tilde{r}; r', \theta', \phi)$ in (28), the particular notation is used to emphasize that ϕ, r' and θ' are held fixed in the integral in (27). The integration with respect to $\tilde{r}$ is considered before the integration for r' and θ'.

The main integral (26) has an integral over θ' over the range $[0, 2\pi)$. Dividing the integral range $[0, 2\pi)$ for θ' into three disjoint regions namely $[0, \phi-\beta)$, $[\phi-\beta, \phi+\beta]$ and $(\phi+\beta, 2\pi)$ with $\beta > 0$, we get

$$I(\phi) = \sum_{j=1}^{K}\sum_{k=1}^{K} \left(J_{jk}^{(1)}(\phi) + J_{jk}^{(2)}(\phi) + J_{jk}^{(3)}(\phi)\right) \tag{31}$$

where

$$\begin{aligned}
J_{jk}^{(1)}(\phi) &= \frac{1}{(2\pi\tau l)^2} \int_0^{\phi-\beta}\int_0^{R_k(\theta')} \exp\left(\frac{-ir'}{\tau}\right) g_{jk}(r', \theta') r' dr' d\theta', \\
J_{jk}^{(2)}(\phi) &= \frac{1}{(2\pi\tau l)^2} \int_{\phi-\beta}^{\phi+\beta}\int_0^{R_k(\theta')} \exp\left(\frac{-ir'}{\tau}\right) g_{jk}(r', \theta') r' dr' d\theta', \text{ and} \\
J_{jk}^{(3)}(\phi) &= \frac{1}{(2\pi\tau l)^2} \int_{\phi+\beta}^{2\pi}\int_0^{R_k(\theta')} \exp\left(\frac{-ir'}{\tau}\right) g_{jk}(r', \theta') r' dr' d\theta'.
\end{aligned} \tag{32}$$

Examine the phase term (in the exponent) of the above integrals. One factor comes from $-\frac{r'}{\tau}$ and the other from $\frac{\gamma_{jk}}{\tau}$ which is present in g_{jk} in (27). Let $\alpha_{jk} = -r' + \gamma_{jk}$ denote the phase term in the above integrals relative to τ. Since we are interested only in the limit as $\tau \to 0$, the essential contribution to the above integrals comes only from regions (in 5D) near the stationary points of

α_{jk} [10, 19]. The partial derivatives of α_{jk} w.r.t. $r, \theta, \tilde{r}, r'$ and θ' are given by

$$\begin{aligned}
\frac{\partial \alpha_{jk}}{\partial r} &= 1 - \tilde{r}\cos(\theta - \phi), \quad \frac{\partial \alpha_{jk}}{\partial \theta} = r\tilde{r}\sin(\theta - \phi), \\
\frac{\partial \alpha_{jk}}{\partial r'} &= \tilde{r}\cos(\theta' - \phi) - 1, \quad \frac{\partial \alpha_{jk}}{\partial \theta'} = -r'\tilde{r}\sin(\theta' - \phi), \text{ and} \\
\frac{\partial \alpha_{jk}}{\partial \tilde{r}} &= -r\cos(\theta - \phi) + r'\cos(\theta' - \phi) - \rho_{jk}.
\end{aligned} \tag{33}$$

Since both r and r' are greater than zero, for $\bigtriangledown \alpha_{jk} = 0$, we must have

$$\tilde{r} = 1, \quad \theta = \theta' = \phi, \quad \text{and} \quad r = r' - \rho_{jk}. \tag{34}$$

By construction, the integrals $J_{jk}^{(1)}(\phi)$ and $J_{jk}^{(3)}(\phi)$ *do not* include the stationary point $\theta' = \phi$, and hence $\bigtriangledown \alpha_{jk} \neq 0$ in these integrals. Using the *higher order stationary phase approximation* [18], both the integrals $J_{jk}^{(1)}(\phi)$ and $J_{jk}^{(3)}(\phi)$ can be shown to be $O(\tau)$ as $\tau \to 0$ and therefore converge to zero in the limit. This leaves us with just the second integral $J_{jk}^{(2)}(\phi)$ which is restricted to the interval $[\phi - \beta, \phi + \beta]$.

As $\beta \to 0$, we may assume that $R_k(\theta')$ is constant over the θ' interval $[\phi - \beta, \phi + \beta]$ and equals $R_k(\phi)$. (Without this assumption, the main result still goes through, but the proof is rather unwieldy.) Hence, the integral $J_{jk}^{(2)}(\phi)$ can be rewritten as

$$J_{jk}^{(2)}(\phi) = \frac{1}{(2\pi\tau l)^2} \int_0^{R_k(\phi)} \exp\left(\frac{-ir'}{\tau}\right) \xi_{jk}(r') r' dr' \tag{35}$$

where

$$\xi_{jk}(r') \equiv \int_{\phi-\beta}^{\phi+\beta} g_{jk}(r', \theta') d\theta'. \tag{36}$$

In (28), the notation for $\gamma_{jk}(r, \theta, \tilde{r}; r', \theta', \phi)$ was used to emphasize that ϕ, r' and θ' were held fixed in the integral in (27). But in order to compute $\xi_{jk}(r')$ in (36), we need the integral over θ' in the interval $[\phi - \beta, \phi + \beta]$. As $\tau \to 0$, the essential contribution to $\xi_{jk}(r')$ comes only from the stationary points of γ_{jk} [18]. Closely following (33) where we computed the gradients of α_{jk}, it can be readily verified that for $\bigtriangledown \gamma_{jk} = 0$ we must have

$$\tilde{r} = 1, \quad \theta = \theta' = \phi, \quad \text{and} \quad r = r' - \rho_{jk}. \tag{37}$$

Let p_0 denote this stationary point. Then

$$\begin{aligned}
\gamma_{jk}(p_0) &= r' - \rho_{jk} = r_{p_0}, \\
f(p_0) &= r_{p_0} = r' - \rho_{jk}
\end{aligned} \tag{38}$$

and the Hessian matrix $\mathcal{H}$ of γ_{jk} at p_0 is given by

$$\mathcal{H}(r, \theta, \tilde{r}, \theta')|_{p_0} = \begin{bmatrix} 0 & 0 & -1 & 0 \\ 0 & r' - \rho_{jk} & 0 & 0 \\ -1 & 0 & 0 & 0 \\ 0 & 0 & 0 & -r^{'} \end{bmatrix}.$$

The determinant of $\mathcal{H}$ equals $r'(r'-\rho_{jk})$ and its signature—the difference between the number of positive and negative eigenvalues—is zero. From the results of the four-dimensional stationary-phase approximation [18], we have as $\tau \to 0$,

$$\xi_{jk}(r') = (2\pi\tau)^2 \frac{\sqrt{r'-\rho_{jk}}}{\sqrt{r'}} \exp\left\{\frac{i}{\tau}(r'-\rho_{jk})\right\} + \epsilon_1(r',\tau) \tag{39}$$

where $\epsilon_1(r',\tau) \leq M_1\tau^{\kappa}$ with $\kappa \geq \frac{5}{2}$ and includes contributions from the boundary. Plugging the value of $\xi_{jk}(r')$ in (35), we get

$$\begin{aligned} J_{jk}^{(2)}(\phi) &= \frac{1}{l^2}\int_0^{R_k(\phi)} \exp\left(\frac{-i\rho_{jk}}{\tau}\right)\sqrt{r'(r'-\rho_{jk})}dr' \\ &\quad + \frac{1}{(2\pi\tau l)^2}\int_0^{R_k(\phi)} \exp\left(\frac{-ir'}{\tau}\right)\epsilon_1(r',\tau)r'dr'. \end{aligned} \tag{40}$$

Since $\frac{\epsilon_1(r',\tau)}{h^2} \leq M\tau^{\frac{1}{2}}$, the second integral converges to zero as $\tau \to 0$. Let $\chi_{jk}(\phi)$ denote the first integral in (40). Note that $l^2 = L$ and ρ_{jk} depends only on ϕ [as can be seen from Equation (29)]. Then

$$\chi_{jk}(\phi) = \frac{1}{L}\exp\left\{\frac{-i}{\tau}\rho_{jk}(\phi)\right\}\int_0^{R_k(\phi)}\sqrt{r'(r'-\rho_{jk})}dr'. \tag{41}$$

Recall the definition of $I(\phi)$ in (25) and its equivalent statement in (31). So far we have approximated $I(\phi)$ by $\sum_{j=1}^{K}\sum_{k=1}^{K} J_{jk}^{(2)}(\phi)$ and $J_{jk}^{(2)}(\phi)$ by $\chi_{jk}(\phi)$ as $\tau \to 0$. For the theorem statement to hold good, it suffices to show that

$$\lim_{\tau\to 0}\sum_{j=1}^{K}\sum_{k=1}^{K}\int_{\phi_0}^{\phi_0+\Delta}\chi_{jk}(\phi)d\phi = \int_{\phi_0}^{\phi_0+\Delta}P(\phi)d\phi. \tag{42}$$

We now consider two cases: first in which $j \neq k$ and the second in which $j = k$.

case (i) : If $j \neq k$, then ρ_{jk} varies continuously with ϕ. The stationary point(s) of ρ_{jk}—denoted by $\tilde{\phi}$—satisfies

$$\tan(\tilde{\phi}) = \frac{y_j - y_k}{x_j - x_k} \tag{43}$$

and the second derivative of ρ_{jk} at its stationary point is given by

$$\rho_{jk}^{''}(\tilde{\phi}) = -\rho_{jk}(\tilde{\phi}). \tag{44}$$

For $\rho_{jk}^{''}(\tilde{\phi})$ to become equal to zero, we must have

$$\tan(\tilde{\phi}) = -\frac{x_j - x_k}{y_j - y_k} = \frac{y_j - y_k}{x_j - x_k} \tag{45}$$

where the last equality is obtained using (43). Rewriting we get

$$\left(\frac{y_j - y_k}{x_j - x_k}\right)^2 = -1 \tag{46}$$

which cannot be true. Since the second derivative cannot vanish at the stationary point ($\tilde{\phi}$), from the one dimensional stationary phase approximation [11], we have

$$\lim_{\tau \to 0} \int_{\phi_0}^{\phi_0 + \Delta} \chi_{jk}(\phi) d\phi = \lim_{\tau \to 0} O(\tau^{\kappa}) = 0 \tag{47}$$

where $\kappa = 0.5$ or 1 depending on whether the interval $[\phi_0, \phi_0 + \Delta)$ contains the stationary point ($\tilde{\phi}$) or not. Hence,

$$\lim_{\tau \to 0} \int_{\phi_0}^{\phi_0 + \Delta} \chi_{jk}(\phi) d\phi = 0 \tag{48}$$

for $j \neq k$.

case (ii) : If $j = k$, then $\rho_{kk} = 0$. Hence

$$\chi_{kk}(\phi) = \int_0^{R_k(\phi)} r' dr' = \frac{R_k^2(\phi)}{2} \tag{49}$$

and

$$\int_{\phi_0}^{\phi_0 + \Delta} \chi_{jk}(\phi) d\phi = \int_{\phi_0}^{\phi_0 + \Delta} \frac{R_k^2(\phi)}{2} d\phi. \tag{50}$$

Combining both case (i) and case (ii) we get

$$\sum_{j=1}^{K} \sum_{k=1}^{K} \lim_{\tau \to 0} \int_{\phi_0}^{\phi_0 + \Delta} \chi_{jk}(\phi) d\phi = \frac{1}{L} \sum_{k=1}^{K} \int_{\phi_0}^{\phi_0 + \Delta} \frac{R_k^2(\phi)}{2} d\phi = \int_{\phi_0}^{\phi_0 + \Delta} P(\phi) d\phi \tag{51}$$

which completes the proof. □

We have shown that the Fourier transform of the CWR of the distance transform has magnitude peaks on the unit circle of spatial frequency [Lemma (1)]. We have then shown that the squared magnitude of the Fourier transform (normalized such that it has overall unit norm) is approximately equal to the density function of the distance transform gradients with the approximation becoming increasingly tight as τ (a free parameter) tends to zero [Theorem (2)]. Consequently, we can make the identification that $\Psi_\tau(u(\theta), v(\theta))$ is a *complex, square-root density* (of gradient orientation) and that spatial frequencies are essentially gradient histogram bins. (Since the Fourier transform values lie mainly on the unit circle, the difference between marginalization w.r.t. the radial parameter and evaluation on the unit circle becomes negligible.)

5 Empirical confirmation of the main result

The first set of empirical results seeks to validate the principal result in this paper. In Figure 2, we show four shapes[1], their associated distance transforms, the Fourier transform of the CWR and finally the comparison between the true density function—where we have denoted (9) as the true density function for the sake of clarity—and the power spectrum of the CWR. As expected, and at a value of $\tau = 0.00004$, we note from visual inspection that the two density functions are qualitatively similar. While obviously anecdotal, these empirical findings buttress the theoretical result proved in the paper.

[1]Two shapes were obtained from Kaleem Siddiqi whom we thank and the other two shapes are from the GatorBait shape database (http://www.cise.ufl.edu/~anand/GatorBait_100.tgz).

While Theorem 2 establishes the principal result, it does not provide much in terms of the approach toward convergence as $\tau \to 0$. Our next set of empirical results examines the convergence as $\tau \to 0$. In Figure 3, we show the convergence patterns of the FFT density for τ taking values in a set. From an initial density at $\tau = 0.001$ which does not bear much resemblance to the true density (see Figure 3 top left), we see gradual improvement and much closer correspondence at $\tau = 0.00004$. A curious transitory pattern can also be discerned as τ is reduced. At $\tau = 0.001$ and 0.0006, we notice very smooth density function estimates at odds with the shape of the true density. For $\tau = 0.0002$ and 0.00004, we notice the emergence of the "Manhattan" skyline in the density estimator. We do not have any explanation for this empirical observation at the present time.

Finally, we plot a scalar figure of merit—the L_1 norm of the difference between the true and estimated densities for two shapes (Figure 4). As expected, the L_1 norm shows a gradual pattern of convergence as τ is reduced. More detailed work (and with arbitrary precision numerics) is required to understand the approach toward convergence.

6 Discussion

We have shown that the power spectrum of the complex wave representation (CWR) of 2D distance transforms approaches the true density function of the distance transform gradients as a free parameter τ (usually identified with Planck's constant in the physics literature) tends to zero. The proof utilizes the higher-order stationary phase approximation, a technique which is well known and widely deployed in the theoretical physics literature but underused in present day image analysis and machine learning. Insofar as the higher-order stationary phase approximation bounds conspire to work in our favor (as they have clearly done in the 2D case), the extension to 3D distance transforms should be straightforward. This connection to density estimation legitimizes the CWR as a viable distance transform shape representation with potential applications in atlas estimation, shape clustering etc. It remains to be seen if CWRs can play a role in general image analysis domains as well.

Acknowledgments

We thank Brett Presnell, Murali Rao, Sergei Shabanov, Baba Vemuri and Alan Yuille for helpful conversations.

References

[1] Blake, A., Zisserman, A.: Visual Reconstruction. The MIT Press (1987)

[2] Bohm, D.: A suggested interpretation of the quantum theory in terms of "hidden variables", I . Physical Review 85, 166–179 (1952)

[3] Bracewell, R.N.: The Fourier Transform and its Applications. McGraw-Hill Science and Engineering, 3rd edn. (1999)

[4] Butterfield, J.: On Hamilton-Jacobi theory as a classical root of quantum theory. In: A. Elitzur, S. Dolev, N. Kolenda (eds.) Quo-Vadis Quantum Mechanics, chap. 13, pp. 239–274. Springer (2005)

[5] Chaichian, M., Demichev, A.: Path Integrals in Physics: Volume I: Stochastic Processes and Quantum Mechanics. Institute of Physics Publishing (2001)

[6] Christensen, G.E., Rabbitt, R.D., Miller, M.I.: Deformable templates using large deformation kinematics. IEEE Transactions on Image Processing 5(10), 1435–1447 (1996)

[7] de Berg, M., Cheong, O., van Kreveld, M., Overmars, M.: Computational Geometry: Algorithms and Applications. Springer, 3rd edn. (2010)

[8] Geiger, D., Yuille, A.L.: A common framework for image segmentation. International Journal of Computer Vision 6(3), 227–243 (1991)

[9] Geman, S., Geman, D.: Stochastic relaxation, Gibbs distributions, and the Bayesian restoration of images. IEEE Transactions on Pattern Analysis and Machine Intelligence 6(6), 721–741 (1984)

[10] Jones, D.S., Kline, M.: Asymptotic expansions of multiple integrals and the method of stationary phase. Journal of Mathematical Physics 37, 1–28 (1958)

[11] Olver, F.W.J.: Asymptotics and Special Functions. A.K. Peters/CRC Press (1997)

[12] Osher, S.J., Fedkiw, R.P.: Level Set Methods and Dynamic Implicit Surfaces. Springer (2002)

[13] Osher, S.J., Sethian, J.A.: Fronts propagating with curvature dependent speed: algorithms based on Hamilton-Jacobi formulations. Journal of Computational Physics 79(1), 12–49 (1988)

[14] Rangarajan, A., Gurumoorthy, K.S.: A Schrödinger wave equation approach to the eikonal equation: Application to image analysis. In: Energy Minimization Methods in Computer Vision and Pattern Recognition (EMMCVPR). pp. 140–153. LNCS 5681, Springer (2009)

[15] Siddiqi, K., Pizer, S. (eds.): Medial Representations: Mathematics, Algorithms and Applications. Computational Imaging and Vision, Springer (2008)

[16] Siddiqi, K., Tannenbaum, A., Zucker, S.W.: A Hamiltonian approach to the eikonal equation. In: Energy Minimization Methods in Computer Vision and Pattern Recognition (EMMCVPR). pp. 1–13. LNCS 1654, Springer-Verlag (1999)

[17] Tu, Z., Chen, X., Yuille, A.L., Zhu, S.C.: Image parsing: Unifying segmentation, detection, and recognition. International Journal of Computer Vision 63(2), 113–140 (2005)

[18] Wong, R.: Asymptotic Approximations of Integrals. Academic Press, Inc. (1989)

[19] Wong, R., McClure, J.P.: On a method of asymptotic evaluation of multiple integrals. Mathematics of Computation 37(156), 509–521 (1981)

[20] Yuille, A.L.: Generalized deformable models, statistical physics, and matching problems. Neural Computation 2(1), 1–24 (1990)

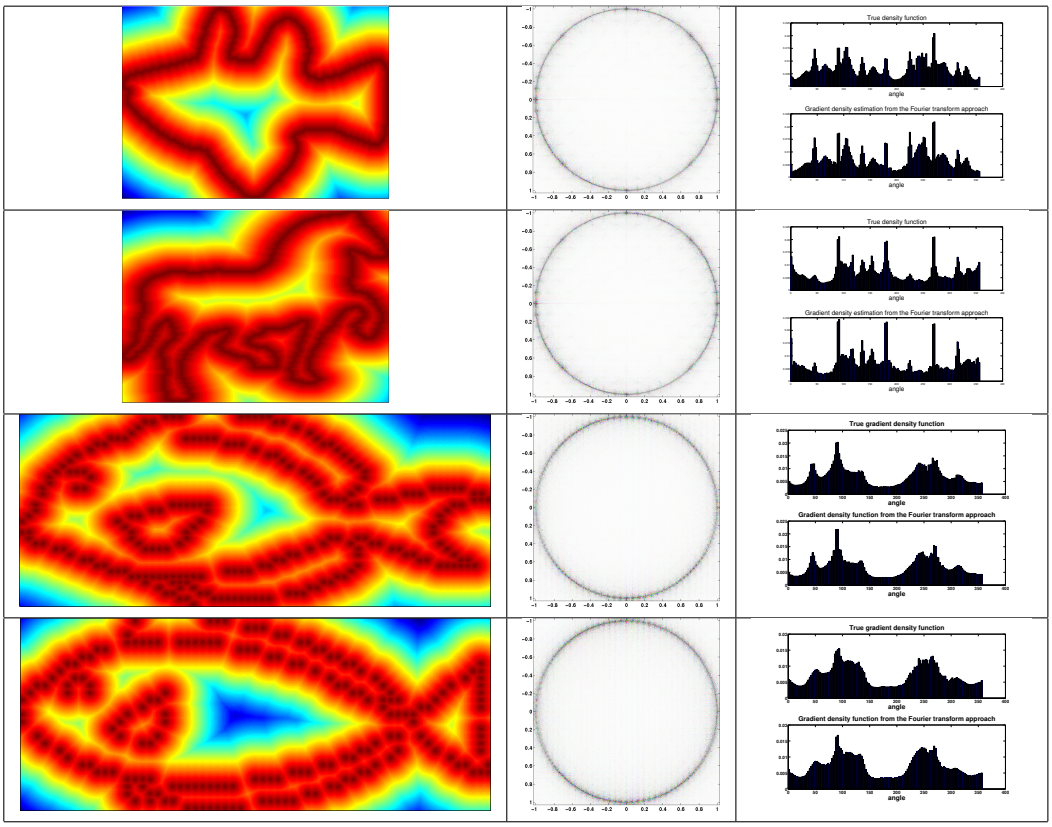

Figure 2: Wave function (left), FFT (middle) and density estimation comparison (right).

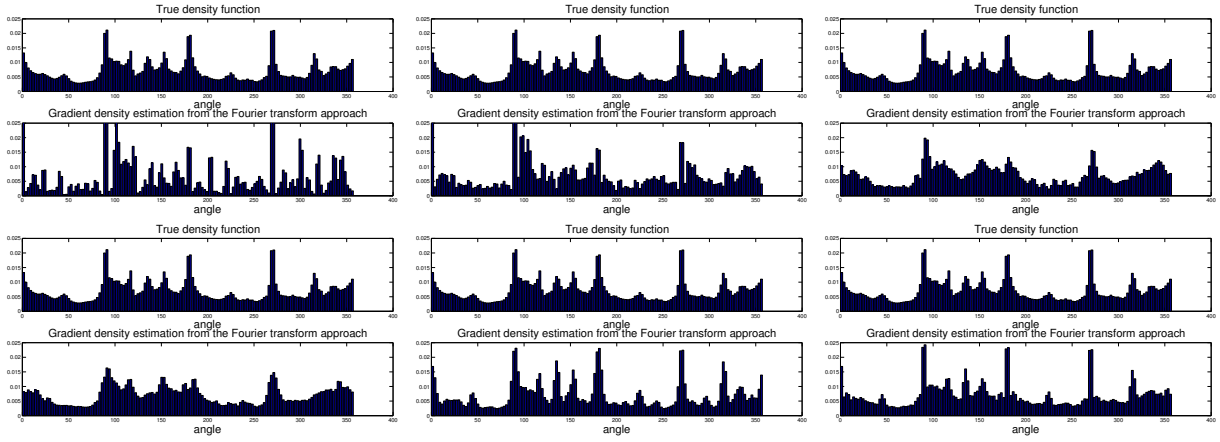

Figure 3: Convergence of the FFT density. Top Left: $\tau = 0.007$. Top Middle: $\tau = 0.004$. Top Right: $\tau = 0.001$. Bottom Left: $\tau = 0.0006$. Bottom Middle: $\tau = 0.0002$. Bottom Right: $\tau = 0.00004$.

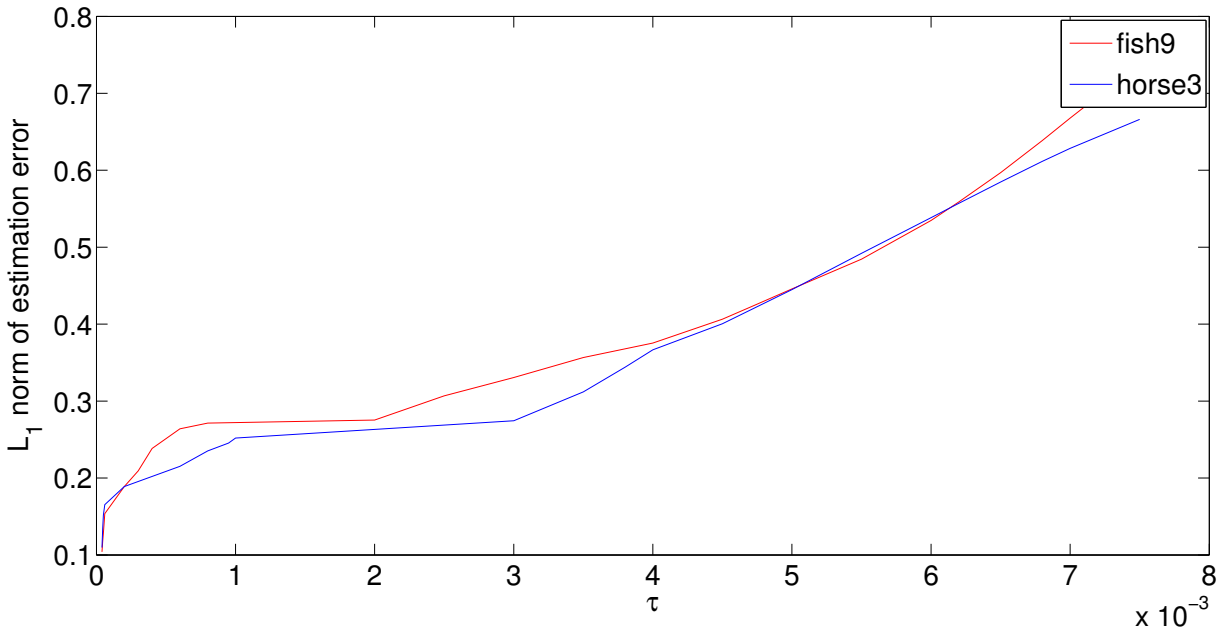

Figure 4: Variation of the L_1 norm of the error with τ for two shapes.